PHYSICAL REVIEW C **84**, 061307(R) (2011)

Decay of the r-process nuclides ^{137,138,139}Sb, and the $A = 130$ solar r-process abundance peak

O. Arndt,[1] K.-L. Kratz,[1] W. B. Walters,[2] K. Farouqi,[1] U. Köster,[3] V. Fedosseev,[4] S. Hennrich,[1] C. J. Jost,[1] A. Wöhr,[2,5] A. A. Hecht,[2,5] B. Pfeiffer,[1] J. Shergur,[2,5] and N. Hoteling[2,5]

[1]*Max-Planck-Institut für Chemie, Otto-Hahn-Institut, Joh.-J. Becherweg 27, D-55128 Mainz, Germany*
[2]*Department of Chemistry and Biochemistry, University of Maryland, College Park, Maryland 20742, USA*
[3]*Institut Laue-Langevin, F-38042 Grenoble, France*
[4]*CERN, CH-1211 Geneva 23, Switzerland*
[5]*Physics Division, Argonne National Laboratory, Argonne, Illinois 60439, USA*

(Received 22 September 2011; revised manuscript received 29 November 2011; published 28 December 2011)

Half-life ($T_{1/2}$) and β-delayed neutron branching (P_n) values of 492(25) ms and 49(8)%, 350(15) ms and 72(8)%, and 93(13) ms and 90(10)% for the r-process nuclei ^{137,138,139}Sb, respectively, have been measured at the CERN On-Line Isotope Mass Separator (ISOLDE) facility by counting β-delayed neutrons. More precise $T_{1/2}$ and P_n values of 300(15) ms and 27(4)%, and 273(7) ms and 50(8)% for ^{136,137}Sn, respectively, have also been measured. The sources were prepared by using the selective ionization of Sb or Sn with the Resonance Ionization Laser Ion Source and the high-resolution mass separator. The new data for Sb isotopes are compared with calculated $T_{1/2}$ and P_n values for both spherical and nonspherical shapes. The data have been incorporated into parametrized nucleosynthesis calculations of the r process in high-entropy winds of core-collapse supernovae in order to study the properties of the $A = 130$ solar-system r-process abundance peak.

DOI: 10.1103/PhysRevC.84.061307 PACS number(s): 23.40.−s, 21.10.Tg, 26.30.Hj, 27.60.+j

The ability to correctly reproduce the $A = 130$ solar-system (SS) isotopic r-process abundance peak, which acts as the main bottleneck in the r-process matter flow, has served as a key test of nucleosynthesis models designed to calculate the total SS r-abundance pattern [1–8]. The quality and usefulness of such calculations have been aided over the past 15 years by the use of newly measured experimental values for a number of the isotopes of Ag, Cd, In, and Sn that lie directly in the path of the r process. Many of those data have been obtained at the CERN On-Line Isotope Mass Separator (ISOLDE) facility through the use of Resonance Ionization Laser Ion Sources (RILIS) to obtain elemental selectivity, in conjunction with high-resolution mass separation to isolate specific isotopes. During that period—with the continuous development and use of RILIS—nuclear-structure properties of ∼25 r-process-relevant isotopes in the $A\sim130$ mass region have been measured including half-lives of 46(7), 158(60), and 35(10) ms for ^{129g,129m,130}Ag, respectively, 242(8), 104(6), 162(7), 68(3), 95(10), and 57(10) ms for ^{129g,129m,130,131,132,133}Cd, respectively, and half-lives of 206(6), 165(3), 141(5), and 92(10) ms for ^{132,133,134,135}In, respectively [9–14]. In this Rapid Communication, new values are reported for the half-lives of ^{137,138,139}Sb obtained through the use of the RILIS tuned for ionization of Sb. More precise half-lives for ^{136,137}Sn are also reported. The use of these chemical ionization and mass-separation techniques for the study of Sn, Sb, and Te nuclei with $A > 130$ is hindered by the increasingly large numbers of β-delayed neutrons (βdn) plus β and γ radiations arising from Cs isotopes that are easily ionized, making β counting for P_n value determinations increasingly difficult. All these experimental data plus optimized theoretical β-decay properties, calculated with the quasiparticle random-phase approximation (QRPA), have been incorporated into parametrized dynamical nucleosynthesis calculations within the so-called high-entropy-wind (HEW) scenario of core-collapse supernovae (for details of the nucleosynthesis model used, see, e.g., Refs. [4] and [7]). In particular, the formation of the $A = 130$ r-process abundance peak has been investigated with this model.

The half-lives were determined by measuring the time dependence of βdn from the Sb parent isotopes using the Mainz Neutron Long Counter in an experimental setup that has been described by Hannawald *et al.* [15], Kautzsch *et al.* [16], and Shergur *et al.* [17]. A new scheme for ionization of Sb was developed at ISOLDE for this experiment. [18,19]. As proton beam pulses from the Proton Synchrotron Booster (PSB) arrive in intervals of 1.2 s, data collection was set to cover a time range of 2048 ms or longer, and to utilize at most every other PSB pulse. The clock for the data collection system was reset by the arrival of a new PSB pulse. The frequency and time range for sample collection were varied to produce sources of reasonable strength and to facilitate the determination of counting rates for the longer-lived isotopes that grew from the radioactive decay of the Sb nuclei and to measure background decay rates.

The βdn counts were binned into 5-ms time intervals, and plotted against the time after the PSB pulse, as shown in Fig. 1 for $A = 137$ with the laser on, and with the laser off. The counts observed with the laser off arise largely from the decay of ^{137}I, produced by surface ionization, which is also a βdn emitter with a 24.1(1)-s half-life and a 7.0(5)% P_n value [20–23]. Similar backgrounds are found at $A = 138$ and 139 from 6.49(7)-s ^{138}I [$P_n = 5.2(4)\%$] and 2.28(1)-s ^{139}I [$P_n = 10.8(12)\%$]. The differences between the counts per time interval obtained with the laser on minus the counts observed with the laser off are subjected to a two-component fit that includes growth and decay of a ^{137}Te component with a P_n value of 3.0(2)%. This fit yields a half-life of 492(25) ms.

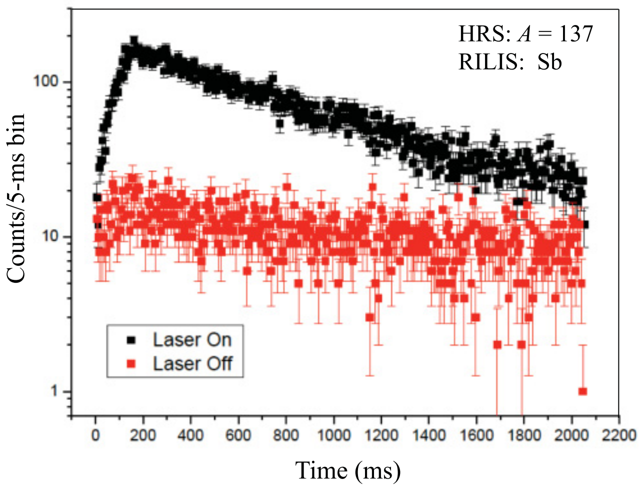

FIG. 1. (Color online) Counts per 5 ms time bin plotted vs the time following a proton pulse from the PSB with the HRS set for $A = 137$. The upper curve (black online) shows data taken with the laser on, and the lower curve (red online) shows data taken with the laser off.

These values are consistent with those reported by Shergur *et al.* of 450(50) ms and a P_n of 49(10)% that emerged from fitting the βdn decay curve for ^{137}Sn decay [24].

The differences between the counts per time interval obtained with the laser on minus the counts observed with the laser off for ^{138}Sb decay are shown in Fig. 2. The fitting process for these data is simplified by the low P_n values and relatively long half-life values for the daughter ^{137,138}Te activities. Using half-life and P_n values of 2.5 s and 3.0% for ^{137}Te, respectively, and 1.4 s and 6.3% for ^{138}Te, respectively, a three-component fit for ^{138}Sb decay yields a half-life of 350(15) ms and a P_n value of 72(8)%.

The difference data for ^{139}Sb decay are shown in Fig. 3. The yield for ^{139}Sb is far lower than for ^{138}Sb, but sufficient

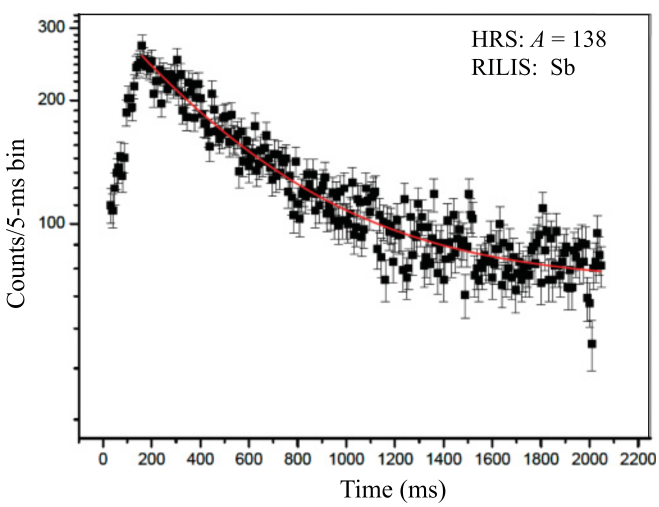

FIG. 2. (Color online) Difference per 5 ms time bin between the counts observed with the laser on and the laser off, plotted vs the time following a proton pulse from the PSB with the HRS set for $A = 138$. The solid line (red online) is a three-component fit to the data yielding a half-life of 350(15) ms.

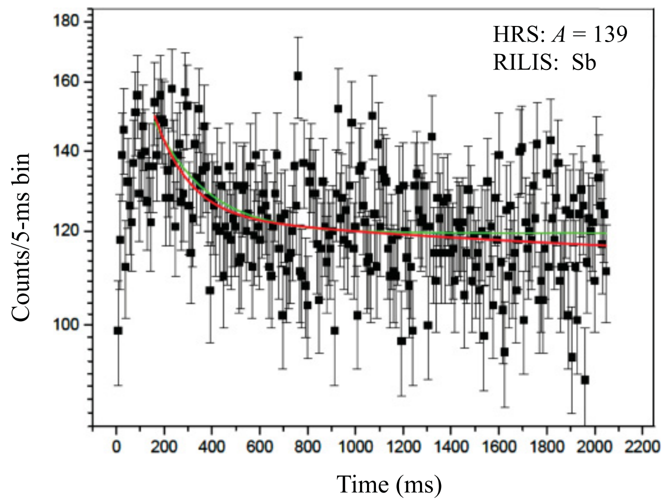

FIG. 3. (Color online) Difference per 5 ms time interval between the counts observed with the laser on and the laser off, plotted vs time following a proton pulse from the PSB with the HRS set for $A = 139$. The solid (thin) line (green online) is a single component fit plus background to the data yielding a half-life of 144 ms. The thicker line (red online) shows a five-component fit that yields a half-life of 93(13) ms.

to extract a half-life of 93(13) ms with a 14% uncertainty. A three-component fit that included only the 1.4-s ^{138}Te daughter and the 6.3-s ^{138}I granddaughter arising from the βdn decay of the parent ^{139}Sb yielded a 93-ms half-life. That value is identical (within uncertainties) to a five-component fit that also included 1.6(3)-s ^{139}Te and 2.28-s ^{139}I. The conclusion is that the P_n value for ^{139}Sb is of the order of 90(10)%.

Subsequent to the experiment in which the half-lives of 250(30) and 190(60) ms were reported for ^{136,137}Sn, respectively, it has been possible to obtain significant improvements in the reduction of background activities at ISOLDE that contribute to the observed spectra [24]. The difference data for ^{137}Sn shown in Fig. 4, were achieved with the RILIS set for Sn under conditions in which a much lower "laser-off" background was observed. Using the newly measured half-life of 492(25) ms for daughter ^{137}Sb, a somewhat longer and more precise half-life of 273(7) ms is extracted from these data for ^{137}Sn, along with a P_n value of 50(10)%. A longer half-life of 300(15) ms has also been determined for ^{136}Sn, with a P_n value of 27(4)%.

These results emphasize the importance of actual measurements for half-lives of nuclei that are expected to be relevant for r-process nuclei that lie near closed shells. At the outset of the experiment, the indirectly determined half-life for ^{137}Sb was 450(60) ms, which turns out to be reasonable with respect to the new value of 492(25) ms [12]. In contrast, earlier QRPA calculations based on the finite-range droplet model (FRDM) masses that only included Gamow-Teller (GT) transitions in the determination of β strength distributions give predictions of 1050, 41, and 179 ms for the half-lives of ^{137,138,139}Sb, respectively, far different from the observed half-lives [25].

The half-lives and P_n values for the neutron-rich Sb nuclei are listed in Table I, along with recently calculated values that include both Gamow-Teller (GT) and first-forbidden (ff)

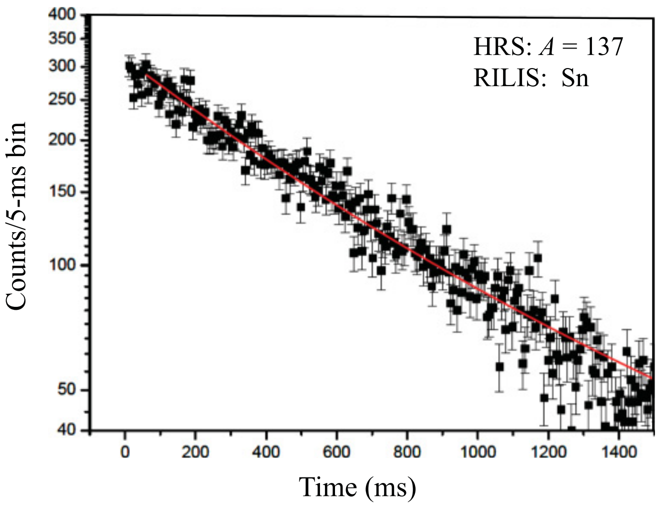

FIG. 4. (Color online) Difference per 5 ms time interval between the counts observed with the laser on and the laser off, plotted vs the time following a proton pulse from the PSB with the HRS set for $A = 137$ and the laser set to ionize Sn. The solid line (red online) shows a three-component fit that yields a half-life of 273(7) ms.

transitions. Literature data for ^{134}Sb isomers are included for comparison with the values for ^{136,138}Sb [26]. The details of these QRPA(GT+ff) calculations are described by Möller, Pfeiffer, and Kratz [27]. The results demonstrate the effects of the possibility of low- and high-spin isomers in odd-odd nuclei. For example, the calculated half-life for ^{134}Sb$_{83}$ of ∼7 s is reasonably close to the measured value for the 10.07(5)-s 7^- isomer, and a factor of 10 too long for the decay of the 0^- ground state. The calculated P_n value for ^{134}Sb$_{83}$ is also consistent with decay of a long-lived, high-spin isomer. For ^{136}Sb$_{85}$, the half-life calculated with nonzero collectivity ($\varepsilon_2 = +0.033$) is 20% larger than the observed value, compared to the spherical calculation ($\varepsilon_2 = 0.0$) that yields a half-life that is longer by a factor of ∼2. For ^{138}Sb$_{87}$, the calculation with nonzero collectivity indicates a low-spin ground state with an open β-decay channel to the ground state of ^{138}Te, whereas the calculation with zero collectivity reflects the expectation of a rather high-spin state, perhaps as high as 8^-, whose direct β decay to lower-energy levels is hindered. The measured value indicates a medium-spin ground state. For ^{135}Sb$_{84}$, collectivity does not appear to play a role, as both calculations, one with $\varepsilon_2 = 0.0$ and the other with $\varepsilon_2 = -0.008$ yield half-lives that are a factor of 2 too long. For both ^{137,139}Sb$_{86,88}$, the calculated values using $\varepsilon_2 = +0.050$ and $+0.092$, respectively, for the Sb parent are slightly larger than the measured values, but are within reason in view of the universal scope of the calculations as seen in Table I. These data show that collectivity, as included in the model via nonzero values for ε_2, becomes important above $N = 84$, as the half-lives calculated using nonzero collectivity tend closer to the observed values, in contrast with those calculated with $\varepsilon_2 = 0.0$.

As the exact astrophysical site and stellar conditions of the r process are still uncertain, a detailed exploration of the systematics of this important nucleosynthesis process in terms of its dependence on nuclear-physics properties far from β stability remains a critical area of investigation. A particularly important mass region in this context is that of the $A \sim 130$ r-process abundance peak, which, owing to the $N = 82$ magic neutron-shell closure, is the dominant bottleneck in the total r-process matter flow. In the past, the majority of such r-process studies have been related to the widely site-independent, classical "waiting-point" approach [28]. In that model the r-process matter flow has been studied under rather simplistic astrophysical conditions, assuming an overall $(n,\gamma) = (\gamma,n)$ equilibrium with several local β-flow equilibria, a constant stellar temperature T, and constant neutron densities n_n in the superpositions of the different n_n components, as well as an instantaneous freezeout [1,5,6,29–31].

Already in the early 1990's, Kratz *et al.* [1] and Thielemann *et al.* [31] pointed out several crucial items for systematic r-process explorations: (i) the potential challenge of learning nuclear structure far from β stability from r-process abundances; (ii) wherever possible, the avoidance of inconsistent sources of nuclear-physics properties; and (iii) the conjecture of a local overestimation of the $N = 82$ shell strength below doubly magic ^{132}Sn in the FRDM mass model [32]. Guided and motivated by these results, not only has a considerable effort been focused on developing new experimental techniques to identify a large number of new, r-process relevant isotopes (the majority of them in the $A \sim 130$ mass region), but also to test in great detail the possible impact of different theoretical models for nuclear masses and gross β-decay properties. The resulting information has been reported in a wide range of publications [1,4–7,14–27,29,31,33].

As a consequence of this work, in more recent years a completely model-consistent nuclear-physics input for the quantities of Q_β, S_n, $T_{1/2}$(GT+ff), P_{xn}(GT+ff), and neutron-capture cross sections deduced from the quenched version of the deformed extended Thomas-Fermi plus Strutinsky

TABLE I. Measured and calculated half-lives and P_n values for neutron-rich Sb nuclei.

Neutron number	83	84	85	86	87	88	89
Isotope	^{134}Sb$_{83}{}^{g}$/^{134}Sb$_{83}{}^{m}$	^{135}Sb$_{84}$	^{136}Sb$_{85}$	^{137}Sb$_{86}$	^{138}Sb$_{87}$	^{139}Sb$_{88}$	^{140}Sb$_{89}$
Half-life (ms)	780(60)/10070(50)	1679(15)	923(14)	492(25)	350(15)	93(+14/−3)	
P_n (%)	0.0/0.088(4)	22(3)	16(3)	49(8)	72(8)	90(10)	
Calculated $T_{1/2}$ ($\varepsilon_2 = 0.0$) (ms)	7490	3327	2000	1265	565	495	364
Calculated $T_{1/2}$ ($\varepsilon_2 \neq 0.0$) (ms)	6960	3301	1103	603	423	150	37
Calculated P_n ($\varepsilon_2 = 0.0$) (%)	0.12	33	40	56	69	87	78
Calculated P_n ($\varepsilon_2 \neq 0.0$) (%)	0.12	34	46	76	73	96	62

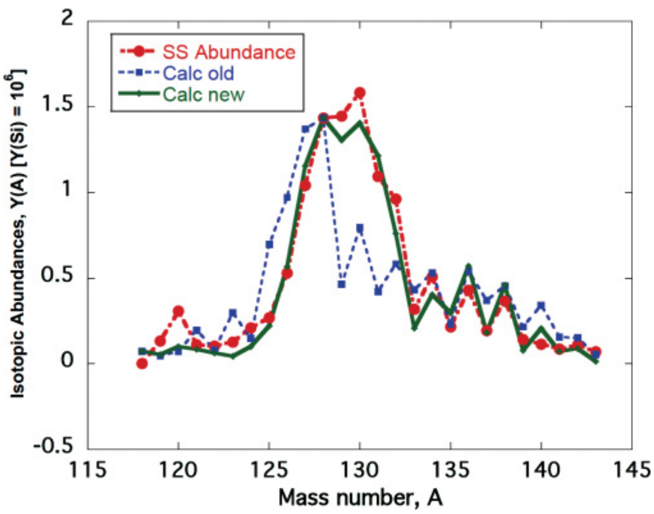

FIG. 5. (Color online) Observed r-process residual isotopic abundances [filled circles connected with a dot-dash line] (red online) along with the values calculated as described in the text using updated half-lives and P_n values [filled diamonds connected with a solid line] (green online), and older half-lives and P_n values [filled squares connected with a dashed line] (blue online). The calculated values are normalized to the abundance of 1.435 for ^{128}Te.

integral (ETFSI) mass model has been used [5,7,30–34]. For comparison, the analogous model-consistent nuclear input from the FRDM mass model, [4–7,25,27,31] and occasionally different versions of the HFB model (up to HFB 17) as well as the Duflo-Zuker mass formula have also been used [35,36].

To illustrate the impact of the new experimental data, the optimized r-process abundance data are plotted in Fig. 5, along with the calculated r-process yields using recently updated input data, as well as with yields calculated using data that were available and in use approximately 10 years ago, using ETFSI-Q masses and first-forbidden β decay [37]. Notice that in this graph the r abundances have been normalized to the r-only isotope, ^{128}Te (in contrast to the often-used normalization to the r-only isotope ^{130}Te), and a linear abscissa has been used where a factor of 2 difference stands out more sharply than in plots that use logarithmic abscissas—see, for example, the plots in Refs. [5–7,30]. The SS r-process isotopic abundance breakdown has been deduced from the recent total SS abundance evaluation of Lodders, Palme, and Gail [38] and the new s-process contributions communicated by Gallino [39]. For the current calculated isotopic r-process abundance data shown for the $A = 130$ peak in Fig. 5, the consistent nuclear-physics input based on the quenched mass model ETFSI-Q [40,41] has been used, and two additional improvements in the nuclear-physics input have been incorporated for the first time. First is the inclusion of the β-decay half-lives of the known $\pi p_{1/2}$ isomers in addition to the $\pi g_{9/2}$ ground-state decays in the two $N = 82$ odd-proton nuclei ^{131}In and ^{129}Ag [10,12,14,42], complemented by theoretical predictions for the lower-Z isotopes ^{125}Rh to ^{123}Tc [43]. The second corresponds to new QRPA(GT+ff) calculations for the local mass region of exotic $83 < N < 87$ r-process isotopes between $Z = 42$ Mo and $Z = 48$ Cd [43]. In these calculations using a spherical Nilsson and BCS model, the relevant κ and μ parameters were optimized to reproduce the experimental level structures of ^{130}In [13] and, in particular, ^{131}In [11,12]. This updated scenario now includes a piece by piece replacement of earlier nuclear-physics input, as well as a change from parameter studies within the site-independent waiting-point model to dynamical calculations within the more realistic, site-specific astrophysical process of the neutrino driven or HEW ejecta of core-collapse supernovae, first suggested in Refs. [44–46], with time variations in neutron density n_n, stellar temperature T, and matter density ρ, and a detailed treatment of the whole freeze-out phase [4,7,43]. As is evident from Fig. 5, with the current best possible input of nuclear data and the choice of appropriate astrophysical conditions for the SN-II HEW scenario, a satisfactory reproduction of the SS r-process isotopic abundance "residuals" of the second r-process peak is possible. Particular attention is drawn to the odd-even effect seen in the r-process "residuals" that is reasonably reproduced in the calculations.

In contrast to the new fit of the r-abundance peak, it can be seen that the use of the older nuclear-physics input data, for example, still used recently by Farouqi *et al.* [7] in the current HEW model, has led to a less satisfactory overall agreement with the SS r-process "residuals". In particular, with the old data the abundances in the rising wing of the peak were overestimated by an average factor of 1.9, whereas the $129 \leqslant A \leqslant 132$ region was underproduced by an average factor of 2.3. Now, with the new nuclear-physics data input, the mass shift in the left wing of the peak is reduced, and the local underabundances at the top of the peak are filled up. Improvements in the new abundance calculations arise from the longer "stellar" half-life of ^{129}Ag (by considering the effect of the $T_{1/2} \sim 160$ ms of the $\pi p_{1/2}$ isomer [10] and the new theoretical P_{xn} values of the most important HEW r-process progenitor isotopes in the $130 \leqslant A \leqslant 134$ mass region, such as $^{130-132}$Pd, $^{130-133}$Ag, and ^{133,134}Cd [43].

In summary, the β-decay half-lives and βdn branching ratios of neutron-rich r-process ^{137,138,139}Sb nuclei have been measured by counting β-delayed neutrons from Sb samples ionized by the ISOLDE resonance ionization laser ion source, and isolated by the high-resolution mass separator. The data from these new measurements have been combined with those from previous measurements to provide experimental half-lives for many of the key r-process waiting-point nuclei associated with the $A = 130$ abundance peak. As a consequence, it is now possible to provide a reasonable fit to both the position and width of the $A = 130$ abundances as well as much of the odd-even staggering on the high-A side of the peak. Both the peak position and width are crucial to the subsequent reproduction of the rare-earth pygmy peak, the third r-process peak at $A = 195$, and the U and Th chronometers. The results of dynamical calculations for isotopic r-process abundances after decay back to β stability, as expected in the HEW scenario of core-collapse SN-II, are presented and found to be in good agreement with the observed SS r "residuals" for the choice of medium neutron freeze-out temperatures of $T_9 \sim 0.85$ and wind velocities of $V_{\exp} \sim 7500$ km/s. Such astrophysical conditions are essential for further r-process matter flow to the rare-earth element pygmy-peak region up to a simultaneous correct fit of the properties of the third r-abundance peak at

$A \sim 195$ (for details, see, e.g., Ref. [7]). Finally, when converting the isotopic r abundances into elemental abundances, as usually measured in metal-poor halo stars [46–50], a reliable reproduction of their abundance patterns for the "main" r process beyond Ba up to the actinide cosmochronometers, can, at present, be fully obtained with parametrized nucleosynthesis calculations as outlined in Ref. [7] and used in the present paper [51].

This work was supported by the US Department of Energy under Grant No. DE-FG02-94-ER40834, and the Bundesministerium für Bildung and Forschung (BMBF) under Contract No. 06MZ-864. The authors wish to acknowledge the support of the ISOLDE staff during the experiments, and during the development of the ionization scheme for Sb. W.B.W. also wishes to acknowledge the support of the Alexander von Humboldt Foundation.

[1] K.-L. Kratz *et al.*, Astrophys. J. **403**, 216 (1993).
[2] K. Takahashi, J. Witti, and H.-T. Janka, Astron. Astrophys. **286**, 857 (1994).
[3] B. S. Meyer, J. Phys. G **19**, 197 (1993).
[4] C. Freiburghaus *et al.*, Astrophys. J. **515**, 381 (1999).
[5] K.-L. Kratz *et al.*, Astrophys. J. **662**, 39 (2007).
[6] B. Pfeiffer *et al.*, Nucl. Phys. A **693**, 282 (2001).
[7] K. Farouqi *et al.*, Astrophys. J. **712**, 1359 (2010).
[8] A. Arcones and G. Martinez-Pinedo, Phys. Rev. C **83**, 045809 (2011).
[9] I. Dillmann *et al.*, Phys. Rev. Lett. **91**, 162503 (2003).
[10] K.-L. Kratz *et al.*, Eur. Phys. J. A **25**, 633 (2005).
[11] M. Hannawald *et al.*, Phys. Rev. C **62**, 054301(2000).
[12] O. Arndt *et al.*, Acta Phys. Pol. B **40**, 437 (2009).
[13] I. Dillmann *et al.*, Eur. Phys. J. A **13**, 281 (2002).
[14] K. Kratz *et al.*, Hyperfine Interact. **129**, 185 (2000).
[15] M. Hannawald *et al.*, Phys. Rev. Lett. **82**, 1391 (1999).
[16] T. Kautzsch *et al.*, Eur. Phys. J. A **9**, 201 (2000).
[17] J. Shergur *et al.*, Phys. Rev. C **71**, 064321 (2005).
[18] R. Catherall *et al.*, Rev. Sci. Instrum. **75**, 1614 (2004).
[19] V. N. Fedosseev *et al.*, Hyperfine Interact. **162**, 15 (2005).
[20] B. Pfeiffer, K.-L. Kratz, and P. Möller, Prog. Nucl. Energy **41**, 39 (2002).
[21] E. Browne and J. K. Tuli, Nucl. Data Sheets **108**, 2173 (2007).
[22] A. A. Sonzogni, Nucl. Data Sheets **98**, 515 (2003).
[23] T. W. Burrows, Nucl. Data Sheets **92**, 623 (2001).
[24] J. Shergur *et al.*, Phys. Rev. C **65**, 034313 (2002).
[25] P. Möller, R. Nix, and K.-L. Kratz, At. Data Nucl. Data Tables **66**, 131 (1997).
[26] A. A. Sonzogni, Nucl. Data Sheets **103**, 1 (2004).
[27] P. Möller, B. Pfeiffer, and K.-L. Kratz, Phys. Rev. C **67**, 055802 (2003).
[28] E. M. Burbidge *et al.*, Rev. Mod. Phys. **29**, 547 (1957).
[29] F.-K. Thielemann *et al.*, Prog. Part. Nucl. Phys. **46**, 5 (2001).
[30] K.-L. Kratz, K. Farouqi, and B. Pfeiffer, Prog. Part. Nucl. Phys. **59**, 147 (2007).
[31] F.-K. Thielemann *et al.*, Nucl. Phys. A **570**, 329 (1994).
[32] P. Möller *et al.*, At. Data Nucl. Data Tables **59**, 185 (1995).
[33] K.-L. Kratz *et al.*, in *Proceedings of the 12th International Symposium on Capture Gamma-Ray Spectroscopy and Related Topics*, edited by A. Woehr and A. Aprahamian, AIP Conf. Proc. No. 819 (AIP, Melville, NY, 2006), p. 409; In *Proceedings of the Carpathian Summer School of Physics 2007*, edited by L. Trache and S. Stoica, AIP Conf. Proc. No. 972 (AIP, Melville, NY, 2008), p. 298.
[34] B. Chen *et al.*, Phys. Lett. B **355**, 37 (1995).
[35] S. Goriely, N. Chamel, and J. M. Pearson, Phys. Rev. Lett. **102**, 152503 (2009).
[36] J. Duflo and A. P. Zuker, Phys. Rev. C **52**, R23 (1995).
[37] Y. Aboussir *et al.*, At. Data Nucl. Data Tables **61**, 127 (1995).
[38] K. Lodders, H. Palme, and H.-P. Gail, in *4.4 Abundances of the elements in the Solar System*, Part of Landolt-Börnstein, Vol. 4B, edited by J. E. Trümper (Springer-Verlag, Berlin, Heidelberg, 2009).
[39] R. Gallino (private communication).
[40] J. M. Pearson, R. C. Nayak, and S. Goriely, Phys. Lett. B **387**, 455 (1996).
[41] P. Möller and K.-L. Kratz (unpublished).
[42] Yu. Khazov *et al.*, Nucl. Data Sheets **107**, 2715 (2006).
[43] K.-L. Kratz and K. Farouqi (unpublished).
[44] S. E. Woosley and R. D. Hoffman, Astrophys. J. **395**, 202 (1992).
[45] B. Meyer *et al.*, Astrophys. J. **399**, 656 (1992).
[46] S. E. Woosley *et al.*, Astrophys. J. **433**, 229 (1994).
[47] I. U. Roederer *et al.*, Astrophys. J. **698**, 1963 (2009).
[48] K.-L. Kratz *et al.*, New Astron. Rev. **48**, 105 (2004).
[49] J. J. Cowan and C. Sneden, Nature (London) **440**, 1151 (2006).
[50] C. Sneden, J. J. Cowan, and R. Gallino, Rev. Astron. Astrophys. **46**, 241 (2008).
[51] A. Frebel and K.-L. Kratz, IAU Symp. **258**, 448 (2008).